Ocean Sci. Discuss., 8, 1757–1775, 2011
www.ocean-sci-discuss.net/8/1757/2011/
doi:10.5194/osd-8-1757-2011

Ocean Science Discussions

Technical Note: Detection of gas bubble leakage via correlation of water column multibeam images

J. Schneider von Deimling[1] **and C. Papenberg**[2]

[1]Leibniz Institute for Baltic Sea Research, Rostock, Germany
[2]Leibniz Institute of Marine Sciences, IFM-GEOMAR, Kiel, Germany

Received: 6 June 2011 – Accepted: 2 July 2011 – Published: 15 July 2011

Correspondence to: J. Schneider von Deimling (jens.schneider@io-warnemuende.de)

Published by Copernicus Publications on behalf of the European Geosciences Union.

Abstract

Hydroacoustic detection of natural gas release from the seafloor has been conducted in the past by using singlebeam echosounders. In contrast modern multibeam swath mapping systems allow much wider coverage, higher resolution, and offer 3-D spatial correlation. However, up to the present, the extremely high data rate hampers water column backscatter investigations. More sophisticated visualization and processing techniques for water column backscatter analysis are still under development. We here present such water column backscattering data gathered with a 50 kHz prototype multibeam system. Water column backscattering data is presented in videoframes grabbed over 75 s and a "re-sorted" singlebeam presentation. Thus individual gas bubbles rising from the 24 m deep seafloor clearly emerge in the acoustic images and rise velocities can be determined. A sophisticated processing scheme is introduced to identify those rising gas bubbles in the hydroacoustic data. It applies a cross-correlation technique similar to that used in Particle Imaging Velocimetry (PIV) to the acoustic backscatter images. Tempo-spatial drift patterns of the bubbles are assessed and match very well measured and theoretical rise patterns. The application of this processing scheme to our field data gives impressive results with respect to unambiguous bubble detection and remote bubble rise velocimetry. The method can identify and exclude the main driver for misinterpretations, i.e. fish-mediated echoes. Even though image-based cross-correlation techniques are well known in the field of fluid mechanics for high resolution and non-inversive current flow field analysis, this technique was never applied in the proposed sense for an acoustic bubble detector.

1 Introduction

Sonar offers a great potential for the remote sensing of the oceans because underwater transmissions of acoustic signals are much more efficient compared to optical ones. Aside from seafloor mapping, echosounders established as standard tools for

OSD
8, 1757–1775, 2011

remote detection of targets such as single fish, fish shoals, zooplankton, or gas bubbles. Small wind/breaker or ship-entrained surficial gas bubbles have been acoustically investigated in detail (Leighton, 1994; Medwin and Clay, 1998). Early publications manifest remote acoustic sensing mainly of methane gas emissions released from the seafloor into the water column (McCartney and Bary, 1965; Merewether et al., 1985). Such methane gas emissions were reported to occur world-wide from virtually all continental margins, estuaries, and river deltas (Judd and Hovland, 2007). The magnitude of these seafloor methane gas emissions and the consideration of potential bubble-mediated flux to the atmosphere, where methane acts as a very strong greenhouse gas, is not well understood (Kvenvolden and Rogers, 2005). Moreover, remote gas bubble sensing and monitoring techniques are needed in regard to future CO_2 sequestration scenarios and potential gas leakages (Oldenburg and Lewicki, 2006).

Progress in digital signal processing brought about the design of so called multibeam systems (De Moustier, 1988) covering large angles (160°) with high resolution (0.5° beam angle). Schneider von Deimling et al. (2007) and Nikolovska et al. (2008) demonstrated its potential for gas seepage mapping. Furthermore modern water column imaging (WCI) multibeam systems are used in obstacle avoidance, bioacoustics, coastal navigation assurance and for scientific seafloor mapping (Gerlotto et al., 2000; Mayer et al., 2002). Best et al.. (2010) demonstrated a PIV cross-correlation approach to extract alluvial flow structures from the water column data of such a new multibeam system.

The use of WCI data of multibeam is hindered by the inconvenient handling of huge amounts of data. Therefore we demonstrate the potential of correlation processing on acoustic multibeam data in regard to bubble detection. An exemplary approach is given to stress efficient gas seepage detection by a datasets gathered in the Baltic Sea at 24 m water depth using a next generation water column imaging (WCI) 50 kHz multibeam system. The proposed processing scheme aims to design a very sensitive, reliable, and automated seep/leak bubble detector.

OSD
8, 1757–1775, 2011

2 Materials and procedures

2.1 Gas bubble acoustics

Gas bubbles in water generally act as a strong acoustic scatterer. The reasons for this are the very large difference in sound speed and density between water and gas, as well as resonance effects controlled by bubble size, frequency, and water depth (Minnaert, 1933; Medwin and Clay, 1998). In our field test (24 m water depth, 50 kHz frequency) we expected scattering in the geometric regime with target strengths (TS) between −65.7 and −40.1 dB, calculated using the non-modal approximation (Medwin and Clay, 1998) for spherical gas bubbles between 1 mm and 20 mm diameter. Thus, even the smallest gas bubbles are expected to backscatter sufficient energy for detection.

Gas bubble hydroacoustics have been studied in detail and the more interested reader is referred to Medwin and Clay (1998), Leighton (1994), and Anderson (1950), who gave the full solution to sound scattering from a fluid sphere in liquid by solving the three-dimensional wave equation.

2.2 Multibeam

A L-3 ELAC Nautik prototype SB3050 was installed with the help of divers below the moonpool of R/V *Poseidon* with a small but mobile $3^\circ \times 2^\circ$ transducer configuration (Mills-Cross). The SB3050 offers a very sophisticated WCI mode (HYDROSTAR WCI Viewer), as was used for online water column inspection. The system transmits three frequency-coded sectors covering 150° swath by 315 equidistant beams. Full water column imaging is available almost in real-time including georeferenced amplitude backscatter values for each beam b and respective time sample s (7 cm). The system was operated with 0.15 ms 50 kHz continuous wave pulse and a ping repetition rate of 0.15 s. Ship motion (roll, pitch, heave, yaw) and ray refraction was compensated to obtain depth z and athwart distance x relative to the transducer. The system

OSD
8, 1757–1775, 2011

automatically corrected the backscatter for absorption and geometrical spreading using a time varied gain. To cover the respective backscatter intensity for gas bubble visualization we selected an optimized color scale and video recording of the data (no raw data access). Finally sonar bitmap images (640 × 433 pixels, 8-bit) with pixel indices x' and z' were generated ($MB(x', z')_t$) for each ping time t.

The multibeam backscatter was not calibrated and thus only relative changes of backscatter intensity were recorded. However, absolute backscattering strength is not necessary for this study.

2.3 Automated bubble detection via PIV

For the proposed bubble detection particle imaging velocimetry (PIV) using cross-correlation was used as post-processing workflow technique for the multibeam sonar images. This method uses cross-correlating of intensity values of images taken at a time interval to generate velocity vectors of individual "seeds" within the images. Bubble-mediated backscatter anomalies are one type of such seeds in sonar images. For more details of PIV methods users are referred to e.g. Raffel et al. (1998).

In Fig. 1 the schematic workflow of the proposed bubble detection is illustrated. Two sonar bitmap images $MB(x',z')_{t1}$ and $MB(x',z')_{t2}$ separated by the ping interval Δt (in our data ($\Delta t = 0.15$ s), respectively, are compared via cross-correlation.

Each bitmap is subdivided into a 9 by 6 matrix (indices i, j) each element representing a respective sub-window or "interrogation-window" (Fig. 1a). For every interrogation window the intensity values at t_1 are compared to the adjacent ones at t_2 within a certain distance (Δx, Δz; Fig. 1b). Maximum correlation values are finally selected (Fig. 1c) to determine the prevailing velocity vector in the respective interrogation-window i, j, that is most readily controlled by moving gas bubbles if present. Since the seeds (bubbles) were not evenly distributed in the data a normalized cross-correlation was applied.

For a better performance, cross-correlation was calculated in the frequency domain (realized with MATLAB *mpiv* toolbox), with the cross-correlation transformed into a

OSD
8, 1757–1775, 2011

complex conjugate multiplication, thus reducing the computational effort from $O[N^4]$ to $O[N^2 \log_2 N]$ operations. Prior to this, inter-frame mean values were subtracted in order to suppress noise with noise-noise or signal-noise mismatch. Subsequent inverse Fourier transformation was used to generate the 2-D-lag-correlogram (Fig. 1c) containing the normalized correlation coefficient R for a given displacement $\Delta x'$ and $\Delta z'$ within the time interval Δt. Peak finding (Fig. 1c) was performed by Gaussian peak-finding algorithm implemented in *mpiv*. By incorporation of water current and bubble rise velocity estimates an "approved zone" of expected bubble lag displacement may be introduced (Fig. 1b, c; black rectangle) as accept/reject parameter. Finally, the gathered pixel lag displacements $\Delta x'$ and $\Delta z'$ were converted into distances (meter) Δx and Δz by the pixel-to-distance relation for the x- and z-direction. By division by the ping interval Δt a two-dimensional velocity vector $\boldsymbol{v}(x,z)$ in $\mathrm{m\,s^{-1}}$ can be calculated for each interrogation-window (i,j).

3 Assessment

3.1 Field site

In the "Mecklenburg Bay" (Baltic Sea, Germany) vast areas are characterized by shallow gas located 2–4 m below the seafloor (Laier and Jensen, 2007). Hydroacoustic evidence of free gas ebullition into the water column was occasionally reported (unpublished results). However, natural gas release into the water column could not be observed during our field test in November 2009. Thus, gas release was artificially induced by lowering a rosette-water sampler system (RWS) on to the gas-charged sediments at 24 m water depth. Subsequently, the rising gas bubbles in the water column were imaged for 75 s, at a fixed position (54°15.109′ N, 11°31.942′ E).

OSD
8, 1757–1775, 2011

3.2 Time slice

In Fig. 2 the backscatter values $MB(x, z)_{t1-3}$ between beam angle −43° and +44° at three different times are presented as color coded "polar" images, with low backscattering plotted bluish and high backscattering plotted yellowish/reddish. High backscatter caused by the seafloor is included in the prominent half-circular side-lobe echoes over all beams. Another artifact plots in the centre beam persistently with elevated backscatter values caused by simultaneous noise affecting the centre beam of the planar array the most by constructive interference after beamforming.

Furthermore Fig. 2a shows the downcast of the RWS in form of a strong backscatter signal in the water column accompanied by side-lobe-echoes in all beams.

A few seconds after the gear had landed on the gassy seafloor, the overload caused some outgassing visible through the escape of individual moving patterns (Fig. 2b, c), which are interpreted as rising gas bubbles squeezed out by load of the RWS on the gas-charged sediments. The bubbles were slightly shifted to the right during the tracking period of a few seconds between Fig. 2b and c. Afterwards, the bubble pattern disappeared from the sonar images.

3.3 Beam slice

In our experiment the vessel stayed at a fixed position and therefore subsequent pings span a 3 vector space temporally. To investigate the rising velocities of gas bubbles we need to analyze their temporal evolution. This is realised by re-sorting the 3-D data cube of consecutive pings in single beam slice images. Each beam slice represents a single beam now imaging travel time against subsequent pings (Fig. 3, beam 31 with 500 pings) and rising gas bubbles emerge very clearly.

During the downcast of the RWS (ping 0–180) some horizontal lines appear between ping 170–280 (Fig. 3 I). This pattern is hardly visible in Fig. 2 and is regarded as neutrally-buoyant gas bubbles detaching from the downcasting RWS. Subsequently rising straight lines plot between ping 330–500 and their rising velocity can be determined

OSD
8, 1757–1775, 2011

from the $\Delta z/\Delta t$ gradient (which was corrected for projecting the travel time of Beam 31 to the centre beam/vertical direction) in Fig. 3 II to v_{z_max} of $-14\,cm\,s^{-1}$ and v_{z_min} of $-34\,cm\,s^{-1}$ (error due to horizontal drift within the beam is neglected because of the narrow beam angle and short range). From ping 400 to 500 the steepness of the gradient and the cease in backscatter intensity indicates smaller bubbles with lower v_z and TS.

The advantage of this display is clearly visible, as it not only shows the bubble trajectories (beam-wise), but also improves visual object detection, because of the signal coherency in consecutive pings. If lateral currents and bubble drift are low compared to their rise velocity then moving bubbles plot more distinctly by presenting *MB* data for a fixed beam over the entire sampling period over all pings (Fig. 3).

3.4 Correlation processing

To sense moving targets in the sonar images PIV was applied to determine the dominating velocities therein. The resulting velocity vectors are presented in Fig. 4. Interrogation-windows (5,4) and (5,5) show distinct negative (upward) v_z. In (7, 3) and (9, 4) some artifacts show up at the boundary of the swath image, however, they do not occur consecutively. Outside of the bubble-influenced area (off-seep) no significant vector components appear in the respective interrogation windows.

To investigate data over a longer period v_z and v_h values were calculated between successive pairs of images $p = 300$ to $p = 400$ and visualized in a compound vector plot for an "on-seepage" interrogation-window (5, 4) and an "off-seepage" (Fig. 5) interrogation-window (6,3). The (5,4) "on-seepage" vectors are strongly biased towards +x- and −z-direction in agreement with bubble movement observed in Figs. 2 and 3. The corresponding lateral displacement values of $+0.2\,m\,s^{-1}$ could not be attributed due to missing current information.

The off-seepage analysis shows neither a bias towards +x/−z-direction nor smaller values of v_z within the seep-indicative v_{z_seep} range defined later. "Off-seep" vectors plotted in Fig. 5 are thus interpreted as derived from noise-noise correlation.

OSD
8, 1757–1775, 2011

4 Discussion

4.1 Seep bubble detection

Natural gas release can be discriminated into minor and major gas release events after Leifer and Boles (2005). Minor gas release is characterized by individual gas bubbles following each other with a narrow Gaussian distributed bubble size spectrum. Typical peak diameter were reported of around ~5 mm at depths up to 1000 m (Leifer and McDonald, 2003; Leifer and Boles, 2005; Sahling et al., 2009; Sauter et al., 2006; Schneider v. Deimling et al., 2011). Terminal rise velocities of such buoyant gas bubbles can be estimated after Clift et al. (1978), e.g. 1 mm to 20 mm large bubbles would rise with v_{z_seep} 0.1–0.35 m s^{-1}.

In contrast major gas releases cause broad bubble spectra ranging between 0.3 mm–50 mm and upwelling flows yield v_z values up to 2 m s^{-1} (Leifer et al., 2006).

To our knowledge gas and/or oil seepage/leakage from the seafloor represents the only mechanism to sustain a continuous production of rising objects with v_{z_seep} in the ocean. Thus, our detection scheme aims to find those "rise patterns" in the data, which are regarded as seep-indicators (v_{z_seep}). Fish represent a main driver for confusion in respect to acoustic bubble investigations, but this confusions can be overcome by consideration of differences in echo trajectories of bubbles and fish (Ostrovsky, 2003, 2009). Even though fish may rise temporarily within the same v_{z_seep} range, persistent detection of v_{z_seep} values clearly points to a gas source on the seafloor.

Available data on oceanographic parameters (e.g. currents) for the time of v_{z_seep} measurements can improve the proposed processing scheme (Fig. 1) considerably through velocity investigations on passively rising bubbles, as pointed out in Schneider von Deimling et al. (2010). If current data is not available an assumption of ocean velocities smaller than <1 m s^{-1} below the mixed layer could be used for setting a threshold.

Stationary acoustic gas bubble monitoring studies (Dworski and Jackson, 1994; Minken and Sevaldsen, 1987; Greinert, 2008) have concentrated on elevated

OSD
8, 1757–1775, 2011

backscatter from bubbles – not their trajectories. However pure backscatter analysis as a gas bubble seep indicator is very vulnerable to fish echoes.

Maximum and mean rise velocities of $v_{z\_min} = -38\,cm\,s^{-1}$ and $v_z = -16\,cm\,s^{-1}$ were gathered with our PIV processing. Both of these values fit very well to both, the manually picked rise velocities and theoretical values for minor seep bubble spectra. At least for low flux gas leakages the rising behavior of gas bubbles lies in a limited range, that can be used for discrimination between rising gas bubbles and other unwanted echo targets.

Improved sonar image or signal processing is needed to ascertain that gas bubbles originate from the seafloor: with increasing beam angle, the prominent half-circular first arrival side-lobe (Fig. 2a) disturbs the water column signal in modern WCI multibeam mapping sonar data. Here, sophisticated PIV methods such as optical flow etc. may be valuable for improved target detection. Signal – in contrast to image-processing of the raw WCI-data at this stage is expensive in computational cost and much pioneering work will be needed to handle the large quantity of WCI data. Nevertheless, basic signal processing of raw WCI data allowed us to geometrically permute our test data and, although not shown in this study, to successfully enhance the signal quality of the raw data signal. Our data was recorded while the vessel was stationary and bubbles were hardly affected by perpendicular lateral currents to the swath. However, the trajectories of echoes caused by buoyant gas bubbles in the water column are three-dimensional in nature. Therefore, a single swath can only ensonify a two-dimensional slice (snapshot) of this three-dimensional volume. By collecting multiple swaths over a period of time a data volume of subsequent pings can be stored. After re-sorting this data to horizontal time/depth-slices a vertically contiguous object is cut into a series of horizontal slices, in which it is now imaged as an isolated object, Thus, it is possible to "trace" the spatially-coherent bubble rise pattern down to the seafloor even if currents have deflected the gas bubbles from one swath into another.

Future multibeam mapping systems may offer athwart swath steering of about 20°. In combination with a high ping rate this would offer repeated insonification of individual

OSD
8, 1757–1775, 2011

gas bubbles during a survey.

Methods are already available to extract the third component of the velocity vector as well (stereo techniques, dual plane PIV: Raffel et al., 1998) and thus allow for tracking a 3-D bubble path. However, the computational effort becomes even higher.

4.2 Limitations

One major constrain in using the proposed correlation processing arises from seeding density and resolution issues. Both, the horizontal and vertical resolution are strongly range dependent. If the distance between individual bubbles (seeds) is significantly smaller than the data resolution, then the acoustic trace of gas seepage plots spatially continuous and the introduced interrogation-windows are not longer seeded with individual particles and PIV might fail. This is especially the case, if a major gas release seeds the water column with variously sized bubbles having very different v_z values. The prototype system in our study is not ideally suited for such tasks given its fairly large pulse length (0.15 ms) and relatively low resolution ($2^\circ \times 3^\circ$, 50 kHz). Application of a high frequency/narrow beam system would offer up to 3 mm vertical resolution and 60 Hz ping rates. Under these conditions the proposed processing scheme is expected to work much better.

A promising step would be the direct application of the detection algorithm on the signal data. Although in this study we have only used signal processing for re-sorting the data to generate beam-slice images, future developments and algorithms can be applied to the raw data directly.

5 Conclusion

With the advent of the next generation WCI multibeam systems water column data become accessible and require new processing techniques. With data of our 50 kHz prototype sounder we successfully developed a method to record the rise pattern of

OSD
8, 1757–1775, 2011

individual gas bubbles released from the seafloor. The applied method is based on correlation techniques adapted from image processing and potentially represents a base for automated seepage/leakage detection. Correlation processing of raw WCI data, in this study tested and only used for geometrical aspects, is a promising tool in future WCI investigations, as the methods adapted from image processing can be directly applied to raw data. With higher frequency systems and sector steering techniques the proposed method will be more sensitive. Our study shows that automated WCI processing in general can potentially be a major asset for a wide range of hydroacoustic applications such as gas seepage analysis, monitoring of man-made subsea installations with special emphasis on low gas flux leakage detection, and ocean current analysis.

Acknowledgements. The authors would like to thank L3-Communications ELAC-Nautik GmbH for supplying the prototype echosounder as well as for system adaption, installation, and support. We greatly appreciate the hardware and funding support of Wilhelm Weinrebe and Gregor Rehder. Special thanks go to the scientific diver team namely Florian Huber, Christian Howe, Nikolaus Bigalke and Björn Thoma for tricky transducer installation and to the crew members of R/V *Poseidon* for their support. We honor the critical proof reading of Ralf Prien and Michael Glockzin. The ship cruise and respective research leading to these results has received funding from the European Community's Seventh Framework Program (FP/2007-2013) under grant agreement no. 217246 (Baltic Gas) and no. 265847 (ECO2).

References

Anderson, V. C.: Sound Scattering from a Fluid Sphere, J. Acoust. Soc. Am., 22, 426–431, 1950.

Best, J., Simmons, S., Parsons, D., Oberg, K., Czuba, J., and Malzone, C.: A new methodology for the quantitative visualization of coherent flow structures in alluvial channels using multibeam echo-sounding (MBES), Geophys. Res. Lett., 37, 1–6, 2010.

Clift, R., Grace, J. R., and Weber, M. E.: Bubbles, Drops, Particles, New York, Academic Press., 380, 1978.

OSD

8, 1757–1775, 2011

De Moustier, C.: State of the art swath bathymetry survey systems, Int. Hydrogr. Rev., 65, 29–38, 1988.
Dworski, J. G. and Jackson, D. R.: Spatial and temporal variation of acoustic backscatter in the STRESS experiment, Cont. Shelf Res., 14, 382–390, 1994.
Gerlotto, F., Georgakarakos, S., and Eriksen, P. K.: The application of multibeam sonar technology for quantitative estimates of fish density in shallow water acoustic surveys, Aquatic Living Resources, 13, 385–393, 2000.
Greinert, J.: Monitoring temporal variability of bubble release at seeps: The hydroacoustic swath system GasQuant, J. Geophys. Res., 113, C07048, doi:10.1029/2007JC004704, 2008.
Judd, A. G. and Hovland, M.: Seabed Fluid Flow, Cambridge University Press, 2007.
Kvenvolden, K. A. and Rogers, B. W.: Gaia's breath–global methane exhalations, Marine and Petroleum Geology, 22(4), 579–590, 2005.
Laier, T. and Jensen, J. B.: Shallow gas depth-contour map of the Skagerrak-western Baltic Sea region, Geo-Mar Lett., 27, 127–141, 2007.
Leifer, I. and Boles, J.: Measurement of marine hydrocarbon seep flow through fractured rock and unconsolidated sediment, Marine Petroleum Geology, 22, 551–568, 2005.
Leifer, I. and MacDonald, I.: Dynamics of the gas flux from shallow gas hydrate deposits: interaction between oily hydrate bubbles and oceanic environment, Earth Planet. Sci. Lett., 210, 411–424, 2003.
Leifer, I., Luyendyk, B. P., Boles, J., and Clark, J. F.: Natural marine seepage blowout: Contribution to atmospheric methane, Global Biogeochem. Cycles, 20, 1–9, 2006.
Leighton, T. G.: The Acoustic Bubble, Harcourt Brace & Company, 1994.
Mayer, L., Li, Y., and Melvin, G. D.: 3D visualization for pelagic fisheries research and assessment, ICES J. Marine Sci., 59, 216–225, 2002.
McCartney, B. S. and Bary, B. M.: Echo-sounding on probable gas bubbles from the bottom of Saanich Inlet, British Columbia, Deep Sea Res., 12, 285–294, 1965.
Medwin, H. and Clay, C. S.: Fundamentals of Acoustical Oceanography, Academic Press, Boston, 1998.
Merewether, R., Olsson, M. S., and Lonsdale, P.: Acoustically Detected Hydrocarbon Plumes Rising From 2-km Depths in Guaymas Basin, Gulf of California, J. Geophys. Res., 90, 3075–3085, 1985.
Minken, H. N. and Sevaldsen, E.: An Acoustic Gas Detector – its Design Principle and Appli-

OSD
8, 1757–1775, 2011

cation. Technical Report, 1987.
Minnaert, M.: On musical air bubbles and the sounds of running water, Philos. Mag., 10, 235–248, 1933.
Nikolovska, A., Sahling, H., and Bohrmann, G.: Hydroacoustic methodology for detection, localization, and quantification of gas bubbles rising from the seafloor at gas seeps from the eastern Black Sea, Geochem. Geophys. Geosyst., 9, Q10010, doi:10.1029/2008GC002118, 2008.
Oldenburg, C. M. and Lewicki, J. L.: On leakage and seepage of CO_2 from geologic storage sites into surface water, Environmental Geology, 50, 691–705, 2006.
Ostrovsky, I.: Methane bubbles in Lake Kinneret: Quantification and temporal and spatial heterogenity, Limnol. Oceanogr., 48(3), 1030–1036, 2003.
Ostrovsky, I.: Hydroacoustic assessment of fish abundance in the presence of gas bubbles, Limnol. Oceanogr. Methods, 7, 309–318, 2009.
Raffel, M., Willert, C., and Kompenhans, J.: Particle Image Velocimetry, Springer, Heidelberg, 1998.
Sahling, H., Bohrmann, G., Artemov, Y. G., Bahr, A., Brüning, M., Klapp, S., Klaucke, I., Kozlova, E., Nikolovska, A., Pape, T., Reitz, A., and Wallmann, K.: Vodyanitskii mud volcano, Sorokin trough, Black Sea: Geological characterization and quantification of gas bubble streams, Marine and Petroleum Geology, 26(9), 1799–1811, 2009.
Sauter, E. J., Muyakshin, S. I., Charlou, J.-L., Schlüter, M., Boetius, A., Jerosch, K., Damm, E., Foucher, J.-P., and Klages, M.: Methane discharge from a deep-sea submarine mud volcano into the upper water column by gas hydrate-coated methane bubbles, Earth Planet. Sci. Lett., 243, 354–365, 2006.
Schneider von Deimling, J., Brockhoff, J., and Greinert, J.: Flare imaging with multibeam sonar systems: Data processing for seep bubble detection, Geochem., Geophys., Geosyst., 8, 1–7, 2007.
Schneider von Deimling, J., Greinert, J., Chapman, N. R., Rabbel, W., and Linke, P.: Acoustic imaging of natural gas seepage in the North Sea: Sensing bubbles controlled by variable currents, Limnol. Oceanogr. Methods, 8, 155–171, 2010.
Schneider von Deimling, J., Rehder, G., McGinnis, D., Greinert, J., and Linke, P.: Quantification of seep-related methane gas emissions at Tommeliten, North Sea, Cont. Shelf Res., 7–8, 867–878, 2011.

OSD
8, 1757–1775, 2011

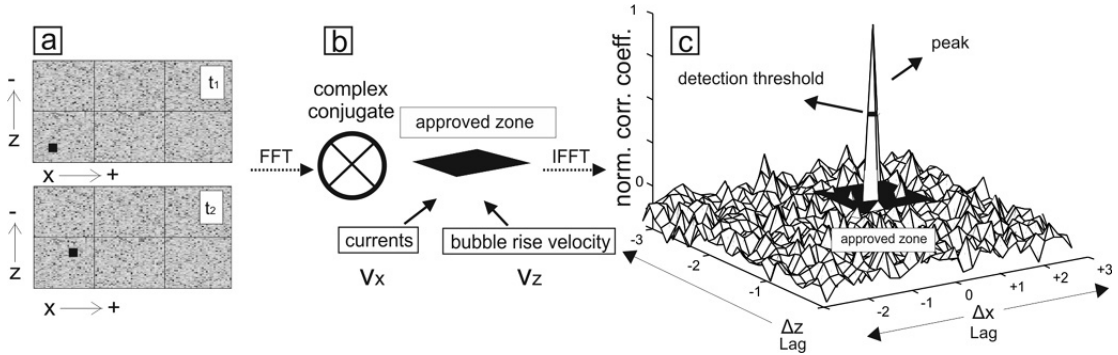

Fig. 1. Schematic diagram illustrating the workflow of a proposed detection algorithm showing **(a)** synthetic echo-images with a solitary "seed" (black rectangle) moving into +x- and +z-direction over time period Δt, **(b)** cross-correlation in the frequency domain and the definition of the "approved zone" controlled by horizontal currents v_x and rise velocity v_z, and **(c)** bubble displacement visible as a Dirac delta peak within the "approved zone" in a 2-D correlogram.

OSD
8, 1757–1775, 2011

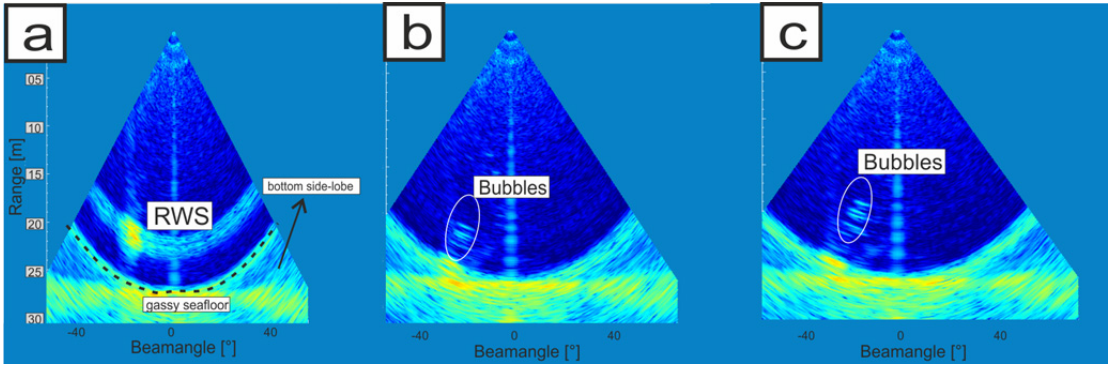

Fig. 2. Color-coded raw backscatter images recorded by the multibeam echo sounder showing background water column reflections (dark blue), centre beam artifact and semicircular side-lobe-interference close to the seafloor (light blue). **(a)** shows the downcast of a rosette-water-sampler (yellowish RWS), **(b)** gas bubble release (yellowish ellipses), and **(c)** vertically shifted gas bubbles. The swath width $x(z)$ at depth covers 41 m, where z represents the water depth minus transducer sea surface installation offset (3.6 m).

OSD
8, 1757–1775, 2011

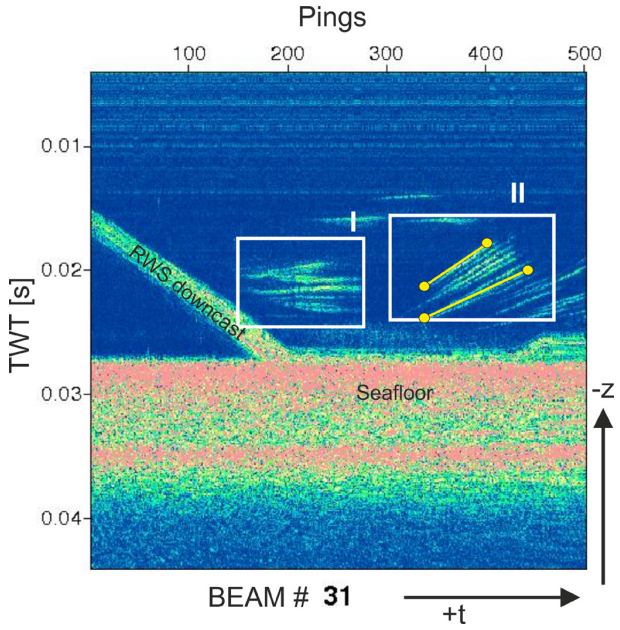

Fig. 3. "Beam slice" presentation with the x-axis representing the ping times (1 ping = 150 ms) and the y-axis showing two-way-travel time for beam 31. The downcast of the rosette-water-sampler (RWS) shows in the left, horizontal straight lines show at $p = 150$ (I), to the right ($p \sim 320$) a compound of rising gas bubbles occur (II).

OSD
8, 1757–1775, 2011

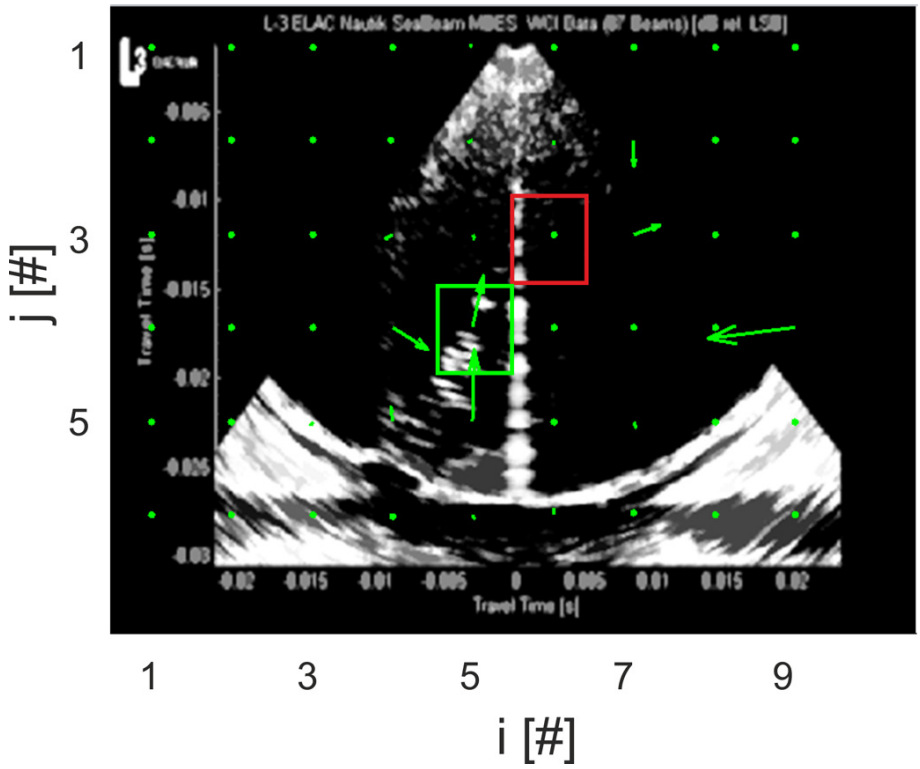

Fig. 4. Mean subtracted image similar to Fig. 2 superimposed with the pixel displacement vector (green arrow) composed of x and z displacements calculated for each interrogation window (i, j). Green and red rectangles indicate the exemplary "on" and "off" seepage interrogation interrogation-window, respectively.

OSD
8, 1757–1775, 2011

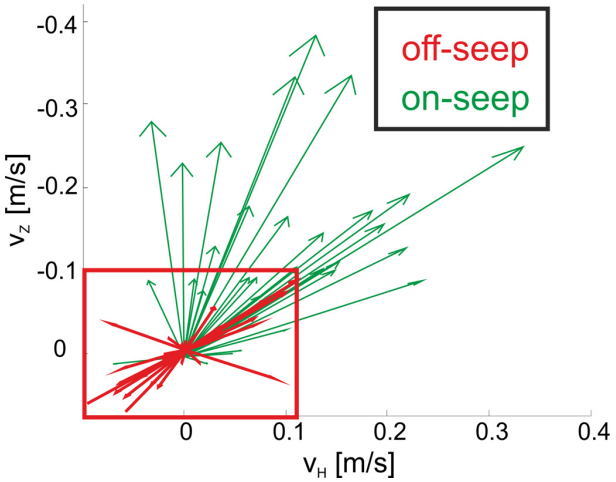

Fig. 5. Velocity vector components v_z and v_h calculated for the "on-seep" interrogation-window (5, 4) and "off-seep" interrogation-window (6, 3) in green and red, respectively. For interrogation-window position see Fig. 4.

OSD
8, 1757–1775, 2011